Experimental investigation of electron heating modes in capacitively coupled radio-frequency oxygen discharge

S K Babu[1], S Kelly[2], S Kechkar[3], P Swift[4], S Daniels[5] and M M Turner[4]

[1] Royal College of Surgeons in Ireland, Dublin, Ireland
[2] School of Chemistry, University College Dublin, Ireland
[3] Intel Corporation Ireland, Collinstown Industrial Estate, Leixlip, Co Kildare, Ireland
[4] School of Physical Sciences, Dublin City University, Ireland
[5] School of Electronic Engineering, Dublin City University, Ireland

E-mail: sharathkumar@rcsi.com

Abstract

A Langmuir probe has been used to investigate electron heating mechanisms in a capacitively coupled oxygen discharge over a wide pressure range (50 – 800 mTorr) at a fixed applied power (200 W). Evidence presented here from experimentally obtained electron energy distribution functions (EEDFs) illustrates discharge transition from collisionless (stochastic) to collisional (ohmic) dominant regime with increasing oxygen pressure. The discharge exhibited a bi-Maxwellian EEDF in the collisionless regime, dominated by stochastic heating whereas Druyvesteyn-like EEDFs in the collisional dominant regime. Moreover, in the transition between these two regimes, parameters such as electron density, effective electron temperature and electron-neutral collision frequency exhibited significant variations.

Keywords: capacitively coupled plasmas, oxygen discharge, Langmuir probe, electron energy distribution function, electron heating

1. Introduction

Radio-frequency (rf) capacitively coupled plasma (CCP) discharges are a key technology in plasma applications for dry etching [1-3] and thin film deposition [4-7]. CCP's are a widespread method for generating technical plasmas where electron populations are heated via modes which are strongly pressure dependent. Technologically relevant plasmas are typically electronegative in nature, however, to date, the pressure dependence of electron behaviour in such important discharges has not been extensively studied experimentally, and is therefore a key motivation for this work. This endeavour is particularly timely as critical dimension in semiconductor devices approach the atomic scale [8] with increasing demand for understanding & control of plasma & surface dynamics.

Variations in gas pressure in an rf discharge can lead to a marked change in the electron heating regime [9]. At moderate to higher pressures electron populations heated via an externally applied rf electric fields deposit energy to other gas constituents through direct collisions. This mechanism of electron heating is often referred as collisional or ohmic where electron collisions resemble resistance heating of a current passing through a conductor. When a discharge is sustained through collisional dominant heating, it is commonly referred as alpha (α) mode which most significantly occurs at moderate to higher pressures with low applied powers/voltages. At large applied power, where significant fraction of power is absorbed by ions which accelerate across the sheath by the large electric field and release secondary electrons, by ion impact on the powered electrode, which can dominate the ionization balance with the discharge is said to be in gamma (γ) mode. In the lowest pressure capacitive discharges, stochastic or collision-less heating becomes important as the electron mean free path extends towards the dimensions of the reactor. Here, electrons can gain additional kinetic energy via momentum transfer from the oscillating plasma boundary sheath [9-11]. This mechanism is key to sustain many low pressure discharges by heating a fraction of the electron population to relatively high energies. Another electron heating mode demonstrated in electronegative

discharges and some molecular discharges is called the drift-ambipolar mode [12, 13] in which electrons are accelerated by strong drift and ambipolar fields at the discharge centre and sheath edges.

The Langmuir probe [14] is the most widely used diagnostic tool for investigating behavior of charged species within a plasma which can be used to understand electron heating. There are numerous reports on the kinetic behavior of electrons using Langmuir probes in various discharges [15-20] and in particular capacitively-coupled plasmas [2, 9-11, 21-28], which is of interest here. Perhaps surprisingly given their widespread use in industrial processes there have been few reports of the kinetic behavior of electrons in oxygen plasmas [25, 26, 29]. Gudmundsson *et al* [30] simulated the evolution of the electron heating mechanism in a capacitively coupled oxygen discharge as a function of pressure using 1-D object oriented particle-in-cell Monte Carlo collision and found ohmic heating to dominate at the plasma bulk at low pressure (10 mTorr) whereas at higher pressures (50-500mTorr), electron heating occurs mainly in the sheath regions. A detailed investigation using a Langmuir probe was carried out recently by Kechkar *et al* [31] who measured electron density, effective electron temperature and electron energy probability function (EEPF) in a capacitively coupled oxygen discharge and showed that any changes in the electron heating mechanism would cause variation in the EEPF measured in the plasma bulk. Importantly that work revealed the threshold power for discharge transition into the γ- mode to be 50 W. Interestingly, with an increase in pressure, the discharge was shown to transit from collisionless to collisional regime at low power (30 W) whereas at higher power (200 W) the transition was from collisionless to γ-mode. However, the pressure variation studies on electron plasma parameters in capacitive oxygen discharge were limited to 200 mTorr due to probe limitations used in that work. The primary aim of this work is to overcome those probe limitations by altering the position of components of probe assembly in the Langmuir probe and measure the variation of plasma parameters such as electron density (n_e), effective electron temperature (T_{eff}) and electron energy distribution function (EEDF) over a wide pressure range for an extended correlation with electron heating mechanism which in turn can further improve the understanding of processing plasmas.

Moreover, transitions in the electron heating mechanism in rf discharge have been shown to be correlated with current-voltage characteristics such as the phase shift angle between current and discharge power. Lisovisky *et al* [32-35] have demonstrated for capacitive discharges that the behavior of these global current-voltage characteristics varies with the electron heating mode. Behavior of these current-voltage characteristics can be monitored using an inline impedance probe positioned below the driven electrode.

In order to gain fundamental insight into key plasma processes, detailed measurements of the pressure dependence of electron populations in capacitively coupled discharges at various is clearly important. To this end, the time averaged EEDF, n_e and T_{eff} were determined for a wide range of pressures (50-800 mTorr) at fixed power (200 W) applied rf power using a Langmuir probe in an oxygen capacitively couple plasma.

2. Experimental tools and diagnostics

In this section details of the plasma reactor is given in section 2.1. Details of the Langmuir probe system utilized is given in section 2.2. Section 2.3 describes a I-V probe which is used to corroborate Langmuir probe measurements.

2.1 Reactive ion etcher - Plasmalab system 100

Figure 1 show a schematic of the Oxford Instruments Plasmalab System 100 [36] rf excited (13.56 MHz) parallel plate capacitively-coupled plasma (CCP) source used in this work. It consists of lower powered/driven electrode and grounded electrode of diameters 205 mm and 295 mm respectively with a 50 mm separation gap. Power was applied to the lower electrode through an auto-match unit. The feedstock gases from the mass flow controller (MFC) unit were fed to the chamber through the shower-head provided on the upper electrode. The reactor walls and electrodes are made of aluminium alloy (6082). An automatic variable throttle valve was located beneath the powered electrode to control the pressure. An Alcatel (ATP400HPC) turbo-molecular pump, with a pumping speed of 400 l/s, was used to evacuate the chamber and backed by an Alcatel rotary pump with a pumping speed of 6 l/s. The MKS (627B-15968) capacitance manometer and Edwards cold cathode ionization (Edwards AIM-S-NW25) pressure gauges

were used with this chamber to measure the process pressure and the base pressure (4.5×10^{-5} to 5×10^{-6} Torr) respectively.

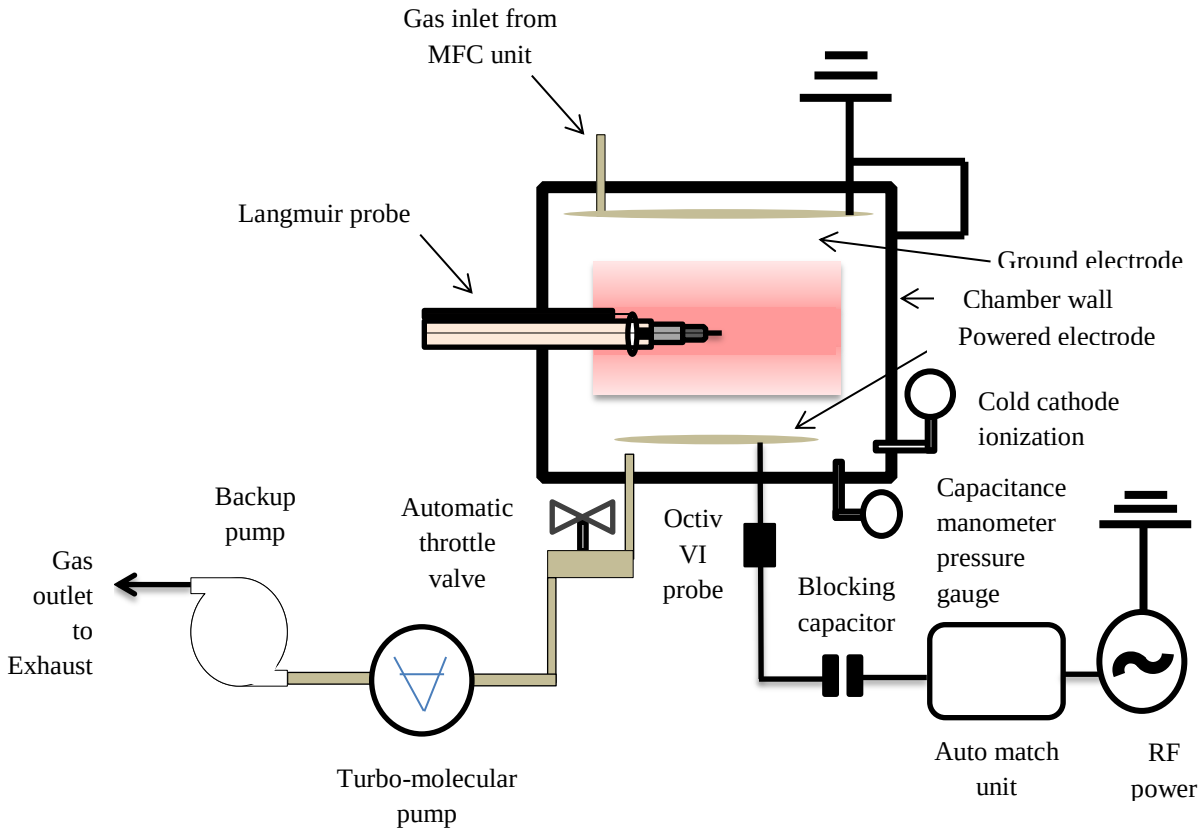

Figure 1 Schematic of Oxford instruments Plasmalab system 100

2.2 Langmuir probe-The SmartProbe

The SmartProbe, which is a commercial Langmuir probe system used in this work, is shown schematically in Figure 2. Developed by Scientific Systems [37], the SmartProbe consists of a Langmuir probe, reference probe with preamplifier, acquisition electronic unit (AEU) and SmartSoft software. The probe tip, which constitutes the active part of the Langmuir Probe, is made of platinum wire with a 0.15 mm diameter and 11.0±0.5 mm in length. The probe is inserted into the chamber from the side and positioned at radial center (2.5 cm above the powered electrode) for most measurements. The advantage of using a platinum wire is to minimize the contamination level preventing distortion of the I-V characteristic. The probe tip is connected to the circuitry through a coaxial cable covered using ceramic shaft as to prevent it making contact with the plasma. The I-V characteristic was obtained by measuring the current drawn by probe at varying probe voltages. The plasma parameters calculated using I-V characteristics assumes that voltage between the probe and the plasma contains only direct current (DC) component and no significant rf component. If there is a contribution from rf component, this would produce distorted I-V data and the plasma parameters measured from this would be incorrect. In order to eliminate the rf component, a compensation electrode along with a set of inductors forms the part of the probe circuitry. The function of this so-called rf compensation is to keep the probe-ground impedance higher in comparison to impedance between the probe and the plasma. To achieve this, a set of self resonant inductors, located close to probe, are tuned to 13.56 MHz and related

harmonics to increase the probe impedance. The inductors were cooled using air through a 4 mm diameter teflon air inlet tube. The SmartProbe also consist of reference electrode (reference probe) which tracks and corrects for any low-frequency or DC shifts in the plasma potential when the probe tip is biased. Low frequency noise, which originates within the discharge due to instability in applied rf voltage, can cause distortion in the probe characteristics [9] as this instability in applied rf voltage can result in the probe voltage noise and drift. The reference probe is made of stainless steel and forms a wire loop around the main shaft of the Langmuir probe. The major part of the reference probe in the plasma was covered with a ceramic shaft for insulation. The other end of the reference probe is connected to probe circuitry through an electrical feed-through. In this work the probe voltage was varied from -95.0 to 95.0 V and the number of samples per point was chosen between 100-200. Moreover, I-V characteristics measured in this work involved an average of 10-20 sweeps. The probe tip was cleaned before each sweep, by biasing the tip at high positive voltage (electron bombardment) for ≈2-3s based on plasma density, to ensure it was free from contamination and changed regularly to minimize the effect of etching by the oxygen discharge.

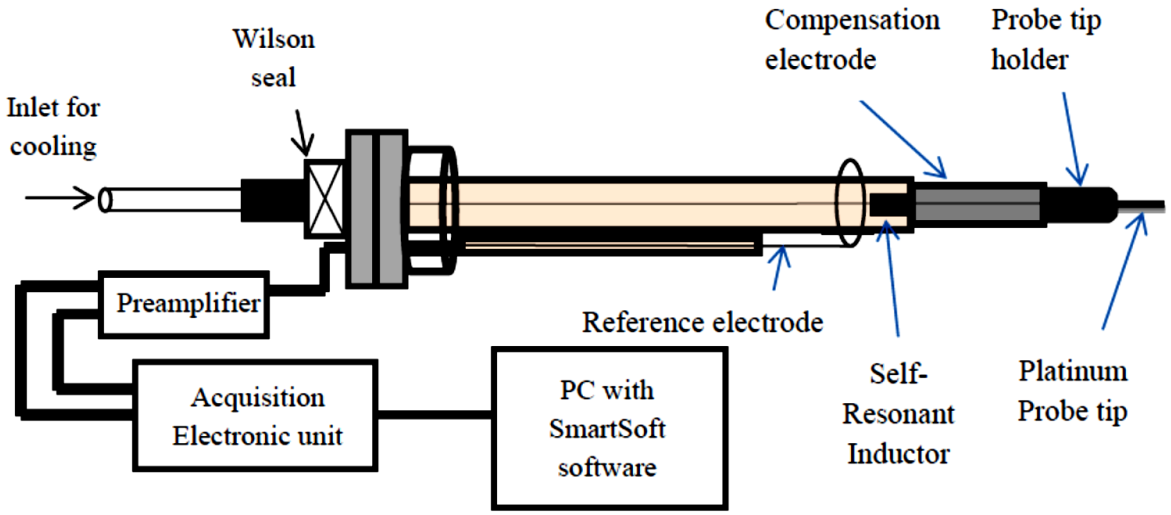

Figure 2 Schematic of the Smart-Probe – commercial Langmuir probe system used in this work.

The Druyvesteyn method [38] was used in this work to determine n_e, T_{eff} and EEDF to allow for non-Maxwellian distributions. Alternative methods often assume a Maxwellian EEDF which can lead to a high degree of uncertainty in the measured plasma parameters in low-pressure discharges [39]. Moreover, this method was successfully employed for previous studies of this discharge [31] and elsewhere [9] for EEDF measurements. The EEDF, $f(\varepsilon)$, obtained using this method is given by,

$$f(\varepsilon) = \left(\frac{d^2I}{dV^2}\right)\frac{2m_e}{e^2A}\left(\frac{2e\varepsilon}{m_e}\right)^{\frac{1}{2}} \quad (1)$$

where ε is the electron energy, I the electron current, V the probe bias, m_e the mass of electron, e the charge of an electron and A is the surface area of probe. The electron density and effective electron temperature can be determined using,

$$n_e = \int_0^\infty f(\varepsilon)\, d\varepsilon \quad (2)$$

$$T_{eff} = \frac{2}{3n_e}\int_0^\infty \varepsilon\, f(\varepsilon) d\varepsilon \quad (3)$$

The electron distribution is often illustrated as an electron energy probability function, $f_e(\varepsilon)$,(EEPF), where,

$$f_e(\varepsilon) = \frac{f(\varepsilon)}{\sqrt{\varepsilon}} \tag{4}$$

The ion current was removed from total current by the procedure described by Steinbruchel [40] to obtain electron current which is required by the Druyvesteyn method to determine EEDF.

2.3 Octiv VI probe

In this work, the phase shift angle between the plasma current and voltage was measured to corroborate Langmuir probe predictions of changes in electron heating mode. An Octiv VI probe developed by Impedance Ltd [41] is employed here. The inline probe was installed the between powered electrode and automatic matching unit. The probe incorporates capacitive sensing for voltage acquisition with inductive current pickups in combination with analogue-to-digital conversion (ADC) circuitry for signal digitisation. The fast Fourier transform is utilised for frequency domain analysis and extraction of phase data via dedicated logic performing noise reduction.

3 Results and discussion

In this section, we present evolution of EEDF in oxygen plasma for a wide range of pressures measured using Langmuir probe to understand the electron heating mechanism. In section 3.1 inline arrangement of a main probe & reference probe/electrode is considered to understand the structures in measured EEDF. In section 3.1.1, investigation of structures in measured EEDF was extended and correlated to positions of reference probe and compensation electrode with respective to main probe tip. Finally in section 3.2 the pressure sensitivity of EEDF's using modified arrangement is presented with analysis of the heating behaviour.

3.1 Investigation of "artificial" structures in measured EEDF

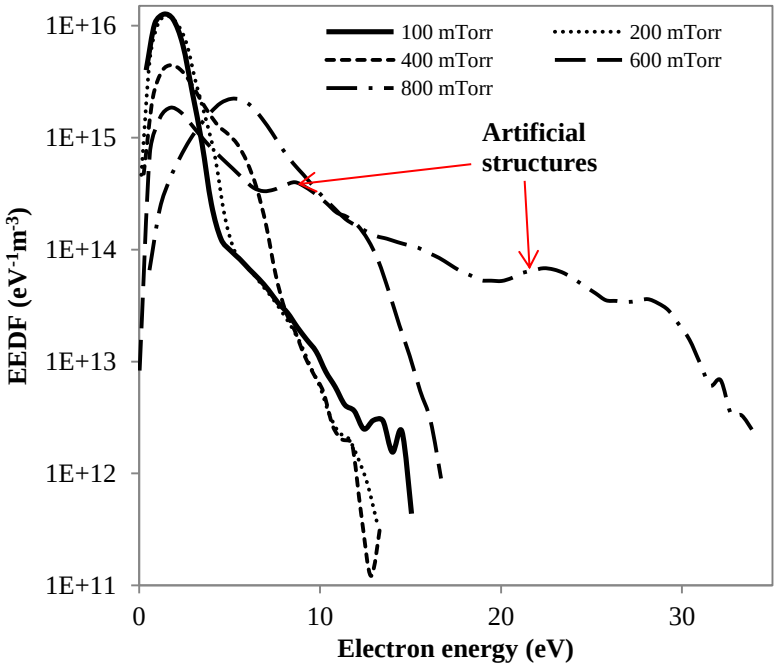

Figure 3 "Artificial" structure(s) observed on EEDFs measured (using standard Langmuir probe setup shown in Figure 4 (a)) as a function of O_2 pressure at 200 W rf power in capacitively-coupled plasma.

In figure 3 we see the evolution of EEDF with increase in oxygen pressure at constant applied rf power of 200 W. As pressure increases a transition to a different electron heating regime is apparent here. At pressures less than 200 mTorr, EEDFs were found to be bi-Maxwellian (see figure 3). Similar bi-Maxwellian characterized EEDFs have been observed previously in capacitive oxygen discharge for pressures less than 100 mTorr [25]. In this scenario the discharge was predominately controlled by stochastic heating, where electrons predominately gain energy from the oscillating rf sheaths at plasma-sheath boundaries [9, 42]. It has been well established in both electropositive discharges of argon [9], helium [9] and electronegative chlorine discharge [43], that ohmic heating dominates with increasing pressure and the EEDF evolves from a bi-Maxwellian to a Druyvesteyn type distribution [8, 49]. In this investigation for pressures greater than 200 mTorr the shapes of EEDFs were found to deviate from bi-Maxwellian indicating that the discharge is clearly in a transition mode. At higher pressures (as the collision frequency increases shown in Figure 9) the plasma bulk tends to become more collisional/resistive. This allows the rf electric field to penetrate into the plasma bulk, where it can heat low energy electrons contained by the ambipolar field. Eventually, with further increase in gas pressure, discharge enters collisional heating regime where ohmic heating is the main power dissipation process and low-electron energy group in plasma bulk are heated by the rf electric field [42].

Here, at oxygen pressures greater than 400 mTorr, "artificial" structures (or dips) were observed in measured EEDFs. Indeed at the highest pressure investigated here (800 mTorr) the high energy EEDF tail is found to increase significantly (as shown in figure 3) which is a behavior not commonly observed in oxygen discharge [25, 30]. It is important to note that this structure or dip in EEPF is different to that usually reported in nitrogen plasma in the energy range of 2-4 eV which corresponds to loss of electrons due to inelastic collisions involving vibrational excitation of the nitrogen molecules [44]. Capitelli *et al.*, [45] reported that super-elastic collisions between electrons and molecules in a metastable state can cause additional peaks or structures in an electron energy distribution. Indeed in capacitive oxygen discharge, metastable molecule $O_2(a^1\Delta_g)$ plays a significant role in the governing heating mechanism [46]. However, no evidence of additional peaks or structure on EEPFs tails in oxygen has been reported to date. This includes computational studies such as the 1-D object-oriented PIC/MCC code 'oopd1', which incorporated the metastable molecule $O_2(a^1\Delta_g)$ along with numerous other species in the reaction set [30, 47]. Appearance of structures and/or high energy tails in EEDF can be possible if there is any distortion in obtained I-V characteristics [9]. This is, therefore investigated extensively in the next section.

3.1.1 Investigating the position of compensation electrode and reference probe

Structures on an EEDF can be the result of distorted probe I-V characteristic and can be caused by such factors as probe contamination, inadequate rf compensation and poor compensation of any low frequency plasma-potential noise and drift [9, 48] due to instability in the rf applied voltage. Distortion of probe I-V data would be possible if any part of probe assembly- the probe tip, probe holder, reference electrode/probe and compensation electrode - is not in the plasma. Here the Langmuir probe arrangement was modified as shown in figure 4 (b) from the standard setup shown in figure 4 (a) to ensure the reference probe always held in plasma bulk so as to avoid any shift in plasma potential due to plasma sheath resistance. In the standard Langmuir probe arrangement shown in figure 4 (a), the wire loop of reference probe is 20 mm in length and is positioned at a distance of ≈ 31 mm from probe tip. At higher oxygen pressures, part of the reference probe in standard Langmuir probe arrangement was visually found to be out of the plasma bulk due to discharge confinement and eventually, fails to accurately account for any changes to plasma potential when probe tip is biased. To verify any distortion to I-V data, the position of reference probe was fixed at the radial center in the plasma bulk, as shown in figure 4 (b) and the main probe (excluding reference probe here) was moved along the radial direction. Structures were observed on measured EEPFs especially at 400 and 600 mTorr for the probe to be furthest away from discharge center shown in figure 5 (b) & (c). With an increase in oxygen pressure, discharge confinement was visually evident. Moreover, asymmetric capacitive oxygen discharges, which are of interest here, are found to become increasingly symmetric with increase in pressure as evidenced by a drop in the dc self-bias voltage [49]. Particularly at 600 mTorr pressure, as the main probe was moved away from discharge center, additional structure began to appear due to the compensation electrode (≈ 15 mm in length and ≈ 24 mm away from probe tip) no longer being in the plasma bulk. When the probe tip was positioned ≈ 30-40 mm

from discharge center, most part of compensation electrode was out of the plasma bulk (which is readily visually observed). It can be concluded that the compensation probe not being in the plasma bulk distorts the measured I-V trace which resulted in additional "artificial" structures at higher energy on measured EEPFs shown in figure 5 (b) & (c).

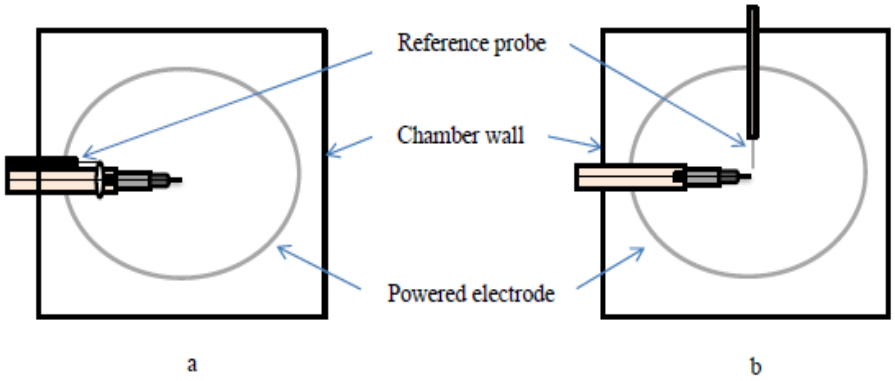

Figure 4 Schematic of Langmuir probe arrangement (a) standard setup used to obtain EEPFs shown in figure 3 ; (b) modified setup with reference probe held close to main probe.

This inadequate referencing to the main probe produced additional structures and/or enhanced tail on EEDF shown in figure 3 due to distorted probe I-V characteristic. Therefore, to improve probe referencing especially at higher pressures, modified Langmuir probe was used for all subsequent data presented here.

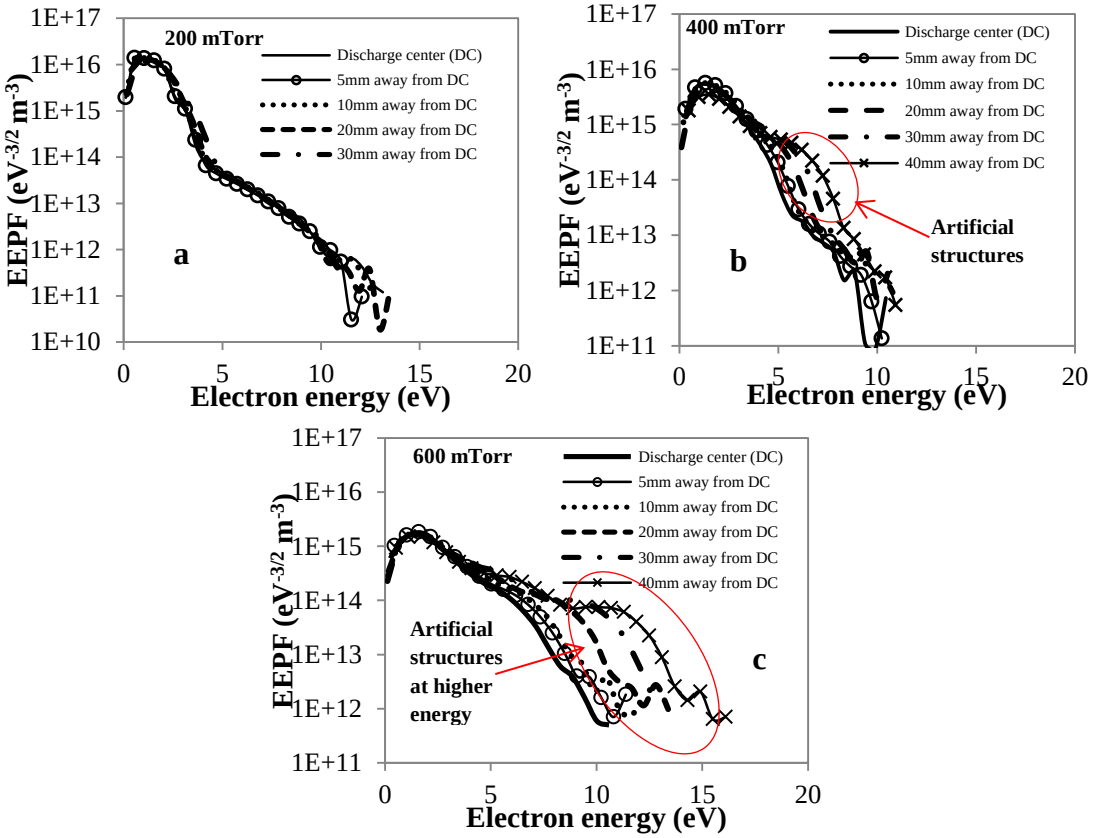

Figure 5 Measured EEPFs as a function of distance from discharge center (DC) in radial direction at (a) 200, (b) 400 & (c) 600 mTorr oxygen pressures operated at 200 W with Langmuir probe set up as in figure 4 (b). Additional

structures and enhanced high energy tails in EEDFs (in 400 & 600 mTorr) caused due to distorted I-V characteristics.

3.2 Investigation of EEDF evolution as a function of O_2 pressure with the modified Langmuir probe arrangement

In this section we investigate EEDFs measured as function of O_2 gas pressures (50-800 mTorr) with the modified Langmuir probe arrangement (as shown in figure 4(b)) for constant applied rf power of 200 W are shown in figure 6 with the corresponding plasma parameters such as electron density and effective electron temperature calculated from the EEDF are shown in figure 7.

3.2.1 Pressures 50-300 mTorr

For pressures in the range 50-300 mTorr, the EEDFs exhibited a bi-Maxwellian shape with low bulk electron temperature (≈0.4-0.5 eV) and high tail energy temperature (≈1-2 eV). A similar bi-Maxwellian characteristic was reported by Lee *et al*., [25] in a capacitive oxygen discharge between pressures 20-100 mTorr and is well known for a capacitively coupled argon discharges at lower pressures [9, 10]. Such EEDF characteristics can result from stochastic dominant electron heating, where electrons are heated by oscillating rf sheaths, which is typical in low-pressure rf discharges [9]. In this heating regime, low energy electrons, with low electron-neutral collision frequency, oscillate without any collisions are unable to gain energy either from weak rf electric field or from the oscillating rf sheaths to overcome the ambipolar potential barrier and are confined in the plasma bulk, whereas the high-energy electron group can overcome ambipolar potential and reach oscillating sheath boundary. Thereby, high-energy electron group gain energy from the collision with oscillating rf sheath boundaries [9, 42].

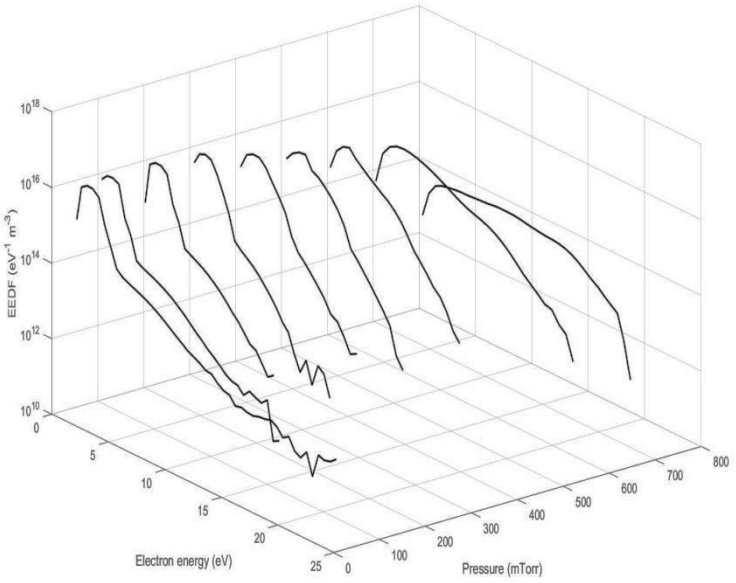

Figure 6 Pressure evolutions of EEDFs measured using Langmuir probe with modified arrangement as in figure 4 (b) in O_2 discharge operated at 200 W applied rf power.

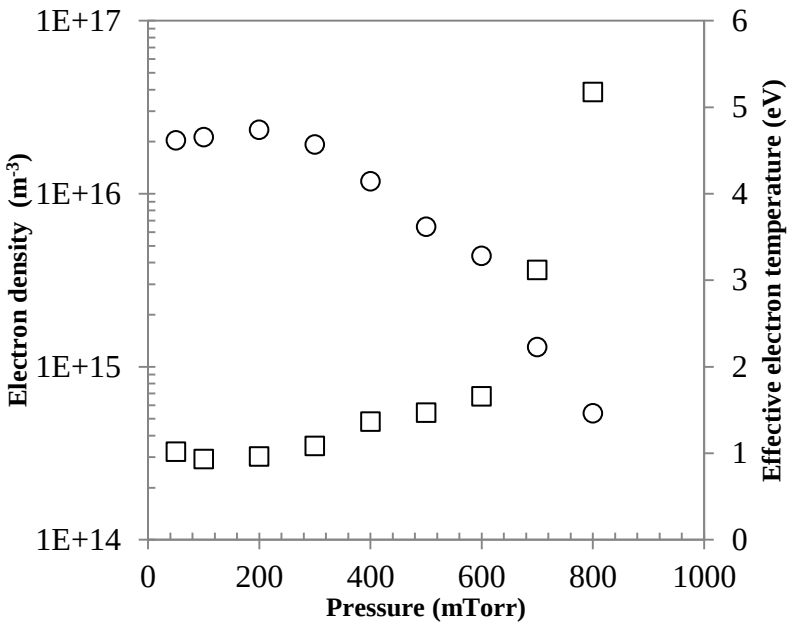

Figure 7 Variations of electron density n_e (○) and effective electron temperature T_{eff} (□) measured using Langmuir probe with modified arrangement as in figure 4 (b) for different gas pressures in O_2 discharge operated at 200 W. Errors due to statistical uncertainties on these measurements arising from uncertainties in the I-V measurements of the Langmuir probe are insignificant and error bars are too small to indicate.

3.2.2 Pressures 400-600 mTorr

An increase in gas pressure results in an increase in electron-neutral collision frequency and therefore, population of high energy electron group decreases, by losing their energy through inelastic collisions, with increasing gas pressures. This is clearly evident in EEDFs for pressures in the range 400-600 mTorr in figure 6. Moreover, the temperature of low-energy electrons, which constitutes to majority (≈ 90%) of electrons in the plasma bulk, found to increase by a factor of approximately 3 as the pressure increased from 200 to 600 mTorr (shown in figure 8). As a result, the shape of EEDFs changed from bi-Maxwellian to Maxwellian distribution for pressures in the range 400-600 mTorr as shown in figure 6 and similar EEDF evolution was reported in capacitively coupled argon discharge [25]. Enhanced electron-electron collisions can also thermalize the electron population towards a Maxwellian distribution in the plasma bulk. This is mostly occurring at large electron densities and lower electron temperatures as electron-electron collision frequency proportional to $n_e T_{eff}^{-3/2}$ allows the EEDF to evolve to a Maxwellian. However, as seen in figure 7, the electron density is found to decrease and T_{eff} increases for pressures in the range 400- 600 mTorr and therefore, evolution to Maxwellian distribution here is less likely due to electron-electron collisions. Another important aspect of EEDF evolution to Maxwellian distribution as gas pressure increases can be collisional ohmic heating of low-energy electrons becoming significant and thereby, low-energy electrons gain sufficient energy to overcome the ambipolar potential field and reach the oscillating sheath to participate in collisionless heating. In contradiction, reports in the literature suggest that collisional heating is inefficient at higher pressures in a capacitively coupled oxygen discharge due to the weak electric field strength [25, 30] and also the reported decrease in the temperature of low-energy electrons with increase in oxygen pressure [25]. However, it has been found here that for pressures above 300 mTorr, the discharge begins to depart from a stochastic heating regime as the temperature of low-energy electrons, determined by the negative inverse slope of linear fit to the data of ln $f_e(\varepsilon)$ vs ε in the electron energy in the range 0.1 to 4 eV, is found to increase significantly (figure 8), due to enhancement of collisional heating. In addition, Lee M.H *et al.* [25] reported a decrease in the density ratio of low-energy electrons to total electrons with an increase in oxygen pressure. Here, ratio of low-

energy electron density, n_{el}, (determined by integrating EEDF in the electron energy range 0.1 to 4 eV) to electron density denoted by R (= n_{el}/n_e) is found to increase only slightly (figure 8), with pressure until 300 mTorr. This small increment is due to contributions from inelastic collisions, however for pressures above 300 mTorr R was found to decrease significantly (shown in figure 8) as low-energy electrons, confined in the plasma bulk, gain sufficient energy to depart from ambipolar potential field due to enhancement of collisional heating. Moreover, an increase in low-energy electron temperature with gas pressure can be due to additional collisional heating. In contrast to this experimental result, simulated results in an oxygen capacitively coupled discharge by Gudmundsson *et al*., [30] reported the opposite trend in EEDF behavior with increase in pressure (10- 500 mTorr) i.e., EEDF changes from Druyvesteyn-like (convex) at low pressures to bi-Maxwellian (concave) at higher pressures. Inconsistency between these two results may be to the fact that experimental measurements reported here were investigated by varying pressure at constant (or fixed) applied power whereas the simulations reported in [30] vary pressure at constant voltage (222 V) which shows more than an order increase in the bulk electron density. This increase in bulk electron density at higher pressures can give an impression that bulk plasma becomes more conductive and easier to screen the rf electric field. Apparently, low energy electrons in their simulations would have not gained enough energy to overcome the ambipolar potential barrier even as pressure increases and therefore, behavior of EEDF transition in their simulations differ to that reported here.

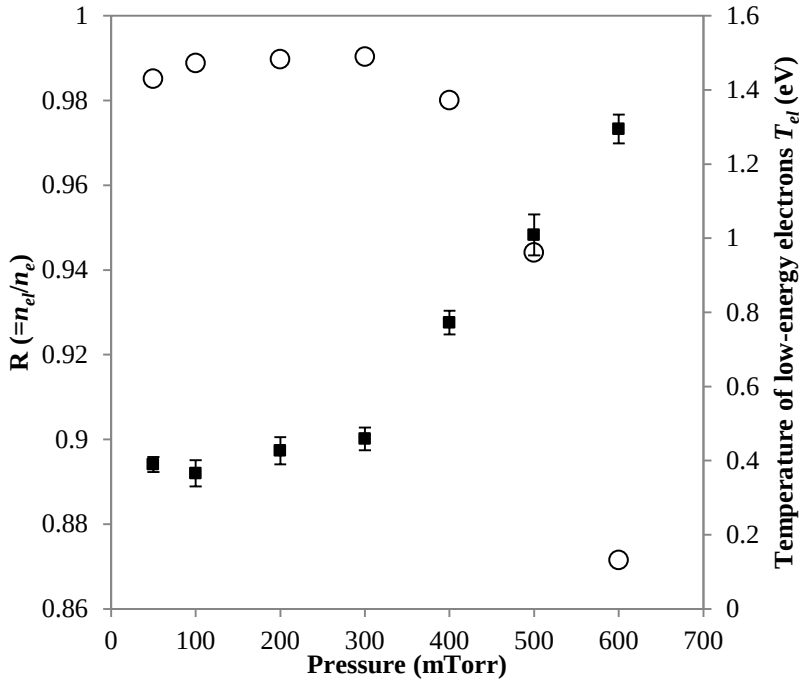

Figure 8 Variations of density ratio of low-energy electron, n_{el}, to total electrons, n_e, R (○) and temperature of low-energy electrons T_{el} (■) with gas pressures in O_2 discharge operated at 200 W measured using Langmuir probe with modified arrangement as in figure 4 (b). Errors bar shown here are calculated using standard error on the slope of a linear fit to the data of ln $f_e(\varepsilon)$ vs ε in the electron energy range with 95% confidence interval.

3.2.3 Pressures above 600 mTorr

At pressures above 600 mTorr the discharge exists in collisional dominated heating regime where ohmic heating is the main rf power dissipation process. Moreover, the effective electron-neutral collision frequency, v_{en}, as shown in figure 9, calculated using,

$$v_{en} = n_g \int_0^\infty \sigma_{en}(\varepsilon)\, f_n(\varepsilon) v(\varepsilon)\, d\varepsilon \qquad (5)$$

is found here to saturate at lower pressures as collisional (ohmic) heating becomes less important. Here v_{en} obtained using normalized EEDF, f_n, momentum transfer collision cross-section, σ_{en}, for oxygen [50] and electron velocity, v. Here, at higher pressures (> 600 mTorr), $v_{en} \gg \omega$ (= 2π×13.56 MHz) for most electrons, therefore the power absorbed by a single electron in the rf electric field of amplitude E is

$$P_{abs} = \frac{e^2}{m_e v_{en}} \times \left(\frac{E}{\sqrt{2}}\right)^2, \quad (6)$$

is equivalent to the power absorption in the dc field. For low-energy electrons, the electron-neutral collision frequency will be small due to smaller electron velocity. Therefore, low-energy electrons are more effectively heated up as the energy gain by the low-energy electrons will be higher than high-energy electrons. Thus, the EEDF evolved close to Druyvesteyn for pressures above 600 mTorr as shown in figure 6 with abrupt raise in T_{eff}.

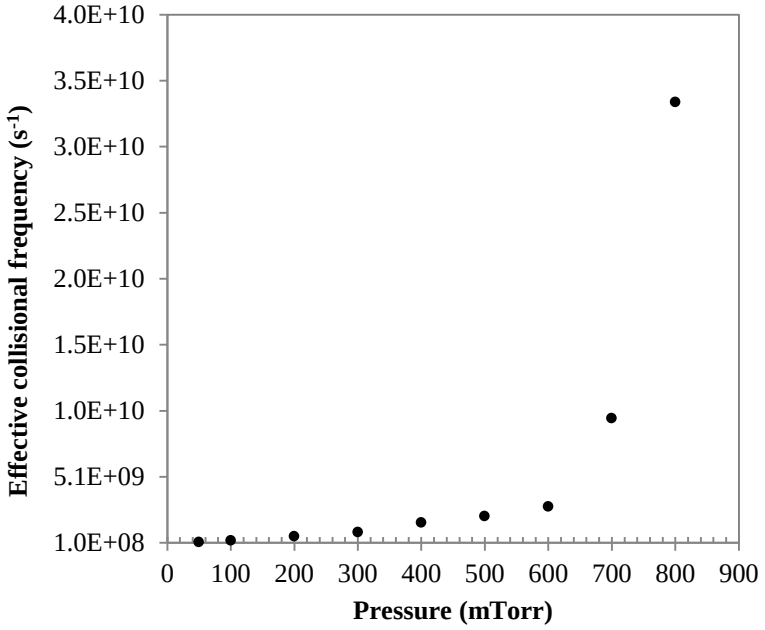

Figure 9 Effective collision frequency calculated as a function of pressure in O_2 discharge operated at 200 W applied rf power.

3.2.4 Phase-shift angle measurements

Additional corroboration of this collisionless to collisional heating mode transition is given by the investigation of the phase shift angle measured using Octiv VI probe shown in figure 10. Two distinct slopes are evident here. A smaller rate of phase change at lower pressures (less than 300 mTorr) indicates a departure from collisional heating. With increase in pressure (>300mTorr), the phase shift decrease indicates $v_{en} \gg \omega$, synonymous with greater rf power dissipation. Lisovskiy *et al* [32] found similar change in phase shift angle which found to decrease with oxygen pressure until it reached the end of α-γ transition in the capacitive oxygen discharge. A more straightforward comparison of phase-shift angle measurements with that of [32] is not be possible here due to facts that gas pressure was varied at constant rf power and discharge limitations. However, it can be derived that at a particular rf voltage, phase shift angle was found to decrease with increasing pressure, as in figure 10, reaching a minimum, where discharge is sustained through ohmic heating mechanism, which can also be referred as collisional or α-mode regime.

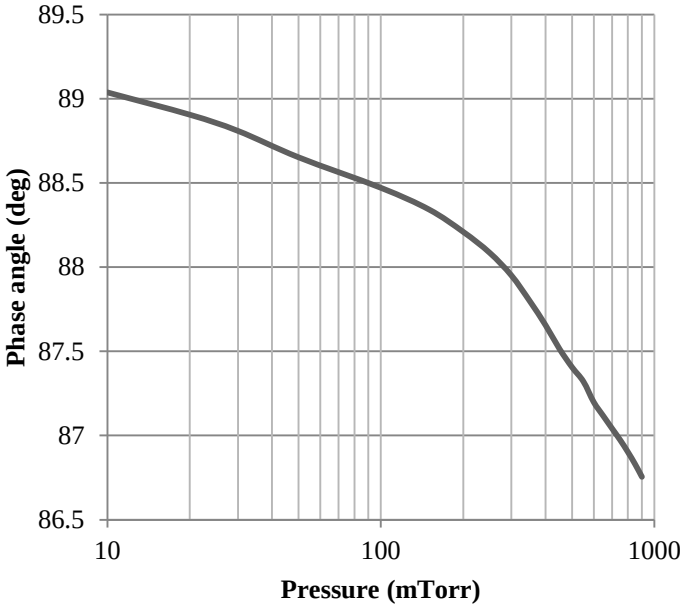

Figure 10 Phase angle measurements using Octiv VI probe for different gas pressures in O_2 discharge operated at 200 W applied rf power. Errors due to statistical uncertainties (standard error on the mean) is of order 10^{-3}.

4 Conclusion

The heating mode transition in a capacitively coupled oxygen discharge using a commercial Langmuir probe has been investigated at greater pressures than have been reported which has been made possible by modification the geometry of the reference probe. The electron heating mode in an oxygen discharge has been found to transit from collisionless to collisional dominant regime with increase in gas pressure and is reported for the first time in a capacitive oxygen discharge. Electron heating transition was marked with bi-Maxwellian shape EEDFs in collisionless regime (50-300 mTorr), Maxwellian EEDFs in the pressure range 400-600 mTorr and Druyvesteyn-like EEDFs in collisional dominant regime (greater than 600 mTorr). Such transition is due to electron behaviors, which at lower pressures gain energy by colliding with oscillating sheath whereas at higher pressures, low energy electrons are heated by rf electric field in the plasma bulk. Moreover, as the discharge begin to deviate from collisionless regime, the temperature of low-energy electrons was found to increase with pressure and the calculated effective electron-neutral collision frequency found to increase by an order magnitude when the discharge exists in collisional dominated regime. Additional corroboration from phase shift angle, measured using a VI probe, which has been found to decrease at faster rate for oxygen pressures $\geq$ 400 mTorr indicating the discharge transition from collisionless to collisional dominated regime.

Acknowledgements

This work was supported by the Science Foundation Ireland under grant No 08/SCR/I1411, the Irish Research Council and Intel Ireland. We would like to thank Mr Conor Murphy for his technical assistance.

References

1. Chabert P and Braithwaite N 2011 *Physics of Radio-Frequency of Plasmas* (New York: Cambridge University Press)
2. Lieberman M A and Litchenberg A J 2005 *Principles of Plasma Discharges and Materials Processing* (NewYork: Wiley)

3. Hartney M A, Hess D W and Soane D S 1989 Oxygen plasma etching for resist stripping and multiplayer lithography *J. Vac. Sci. Technol. B* **7** 1
4. Ertel S I, Ratner B D and Horbett T. A 1990 *J. Bio Mat. Research A* **24** 1637
5. Creatore M, Palumbo F and d'Agostino R *Plasma and Polymers* **7** 291
6. Burns G P, Baldwin I S, Hastings M P and Wilkes J G 1989 *J. Appl. Phys.* **66** 2320
7. Shiomi H 1997 *Jpn. J. Appl. Phys.* **36** 7745
8. Adamovich, I., et al. 2017 *J. Phys. D: Appl. Phys.* 50 323001.
9. Godyak V A, Piejak, R B and Alexandrovich B M 1992 *Plasma Sources Sci. Technol.* **1** 36
10. Turner M M, Doyle R A and Hopkins M B 1993 *Appl. Phys. Lett.* **62** 3247.
11. Deegan C 1999 *PhD Thesis* School of Physical Sciences, Dublin City University
12. Schulze J, Derzsi A, Dittmann K, Hemke T, Meichsner J and Donko Z 2011 *Phys. Rev. Lett* **107** 275001
13. Gudmundsson J T, Snorrason D I and Hannesdottir H 2017 *Plasma Sources Sci. Technol*. **27** 025009
14. Mott-Smith, H.M.and Langmuir, I., (1926), "The theory of collectors in gaseous discharges", *Physical review*, Vol.28 (4), pp. 727.
15. Gudmundsson J T, Kimura T and Lieberman M A 1999 *Plasma Sources Sci. Technol*. **8** 22
16. Gudmundsson J T, Markhtanov A M, Patel K K, Gopinath V P and Lieberman M A 2000 *J. Phys. D: Appl. Phys.* **33** 1323
17. Tuszewski M, Scheuer J T and Tobi J A 1995 *J. Vac. Sci. Technol. A* **13** 839-42
18. Barnes M S, Foster J C and Keller J H 1993 *Appl. Phys. Lett.* **62** 2622-4
19. Schwabedissen A, Benck E C and Robers J R 1997 *Phys. Rev. E* **55** 3450-9
20. Sugai H, Ghanashev I, Hosokawa M, Mizuno K, Nakamura K, Toyoda H and Yamauchi K 2001 *Plasma Sources Sci. Technol.* **10** 378
21. Godyak V A, Piejak, R B and Alexandrovich B M 1992 *Phys. Rev. Lett*. **68** 40
22. Melzer A, Flohr R and Piel A 1995 *Plasma Sources Sci. Technol*. **4** 424
23. Deegan C M, Goss J P, Vender D and Hopkins M B 1999 *Appl. Phys. Lett.* **74** 1969-71
24. Gahan D, Dolinaj B and Hopkins M B 2008 *Plasma Sources Sci. Technol*. **17** 035026
25. Lee M-H, Lee H-C and Chung C-W 2010 *Phys. Rev. E* **81** 046402
26. Pulpytel J, Morscheidt W and Arefi-Khonsari F 2007 *J. Appl. Phys*. **101** 073308
27. Gahan D, Daniels S, Hayden C, O'Sullivan D and Hopkins M B 2011 *Plasma Sources Sci.Technol.,* **21** 015002
28. Scanlan J V and Hopkins M B 1992 *J. Vac. Sci. Technol. A* **10** 1207-1211
29. Liu J, Wen D-Q, Liu Y-X, Gao F, Lu W-Q and Wang Y-N 2013 *J. Vac. Sci. Technol. A* **31** 061308
30. Gudmundsson J T and Ventejou B 2015 *J. Appl. Phys*. **118** 153302
31. Kechkar S, Swift P, Kelly S, Kumar S, Daniels S and Turner M 2017 *Plasma Sources Sci. Technol.* **26** 065009
32. Lisovskiy V A and Yegorenkov V D 2004 *Vacuum* **74** 19
33. Lisovskiy V, Booth J-P, Landry K, Douai D, Cassagne V and Yegorenkov V 2006 Phys. Plasmas **13** 103505
34. Lisovskiy V A 1998 Tech. Phys. **43** 526
35. Lisovskiy V, Booth J-P, Jolly J, Martins S, Landry K, Douai D, Cassagne V and Yegorenkov V 2007 J. Phys. D: Appl. Phys. **40** 6989
36. Oxford Instruments https://www.oxford-instruments.com/
37. Scientific Systems http://www.jcmueller.de/pdf/Smartprobe_brochure.pdf
38. Druyvesteyn M J 1930 *Z. Phys.* **64**, 781
39. Godyak V A, Piejak R B and Alexandrovich B M 1993 *J. Appl. Phys.* **73** 3657
40. Steinbrüchel C 1990 *Journal of Vacuum Science & Technology A* **8** 1663-1667
41. Impedans Ltd https://www.impedans.com/
42. Godyak V A, and Piejak, R B 1990 *Phys. Rev. Lett*. **65** 996
43. Huang. S and Gudmundsson J T 2013 *Plasma Sources Sci. Technol.,* **22** 055020
44. Abdel-Fattah E, Bazavan M and Sugai H 2011 *J. Appl. Phys.* **110** 113303
45. Capitelli M, Colonna G, De Pascale O, Gorse C, Hassouni K and Longo S 2008 *Plasma Sources Sci. Technol.,* **18** 014014
46. Gudmundsson J T and Lieberman M A 2015 *Plasma Sources Sci. Technol.,* **24** 035016
47. Gudmundsson J T, Snorrason D I and Hannesdottir H 2018 *Plasma Sources Sci. Technol.,* **27** 025009
48. Godyak VA and Demidov V I 2011 *J. Phys. D: Appl. Phys.* **44** 233001

412 49. Czarnetzki U, Schulze J, Schungel E and Donko Z *Plasma sources Sci. Technol.* **20** 024010
413 50. Vahedi V and Surendra 1995 *Computer Physics Communications* **87** 179